Fast Computational E-field Dosimetry for Transcranial Magnetic Stimulation using Adaptive Cross Approximation and Auxiliary Dipole Method (ACA-ADM)

Supplemental Material

Dezhi Wang[a], Nahian I. Hasan[a], Moritz Dannhauer[b], Abdulkadir C. Yucel[c] and Luis J. Gomez[a]

[a]Elmore Family School of Electrical and Computer Engineering, Purdue University, IN 47906, USA
[b]National Institute of Mental Health (NIMH), National Institute of Health (NIH), MD 20892, USA
[c]School of Electrical and Electronic Engineering, Nanyang Technological University, 639798 Singapore

Emails: wang5355@purdue.edu, hasan34@purdue.edu, moritz.dannhauer@nih.gov, acyucel@ntu.edu.sg, ljgomez@purdue.edu
#Corresponding Author: Luis J. Gomez
Address: 512 Northwestern Ave, Wang Hall 3007, West Lafayette, IN 47906, USA
Email: ljgomez@purdue.edu
Phone: +001-954-816-5011

S.1 Details of ROIs and coil positions for the cases in Fig. 2

As mentioned in the paper, the ROIs are chosen as the gray matter contained in spherical regions with center $\boldsymbol{r}_{ROI}$ and diameter $\boldsymbol{d}_{ROI}$. The details of the parameters determining the ROIs (center and diameter) are given in Table S1. For the spherical head, as shown in Fig. S1 (A) and (B), the center of the ROI was set at the surface of the inner sphere, and the region inside the inner sphere was chosen as the ROIs, containing 60 tetrahedra for 10 mm diameter and 259 tetrahedra for 20 mm diameter. For the Ernie head model, as shown in Fig. S1 (C) and (D), the center of the ROI was set in the precentral gyrus, and the region inside the gray matter was chosen as the ROIs, containing 412 tetrahedra for 10 mm diameter and 2535 tetrahedra for 20 mm diameter.

Coil positions were chosen by extracting mesh nodes on the scalp that were within a 50 mm diameter of the point on the scalp closest to the center of the brain ROI and then projecting the nodes 5 mm outward in direction normal to the scalp surface [1]. 963 positions are used for spherical head model and 6163 positions are used for the Ernie head model.

Table S1: ROI details and coil numbers for the cases in Fig. 2

	ROI Center (mm)	**ROI Diameter (mm)**	**ROI Tetrahedra Number**	**Coil Number**
Spherical Head	(0,0,70)	10	60	963
		20	259	963
Ernie Head	(-35,-32,86)	10	412	6163
		20	2535	6163

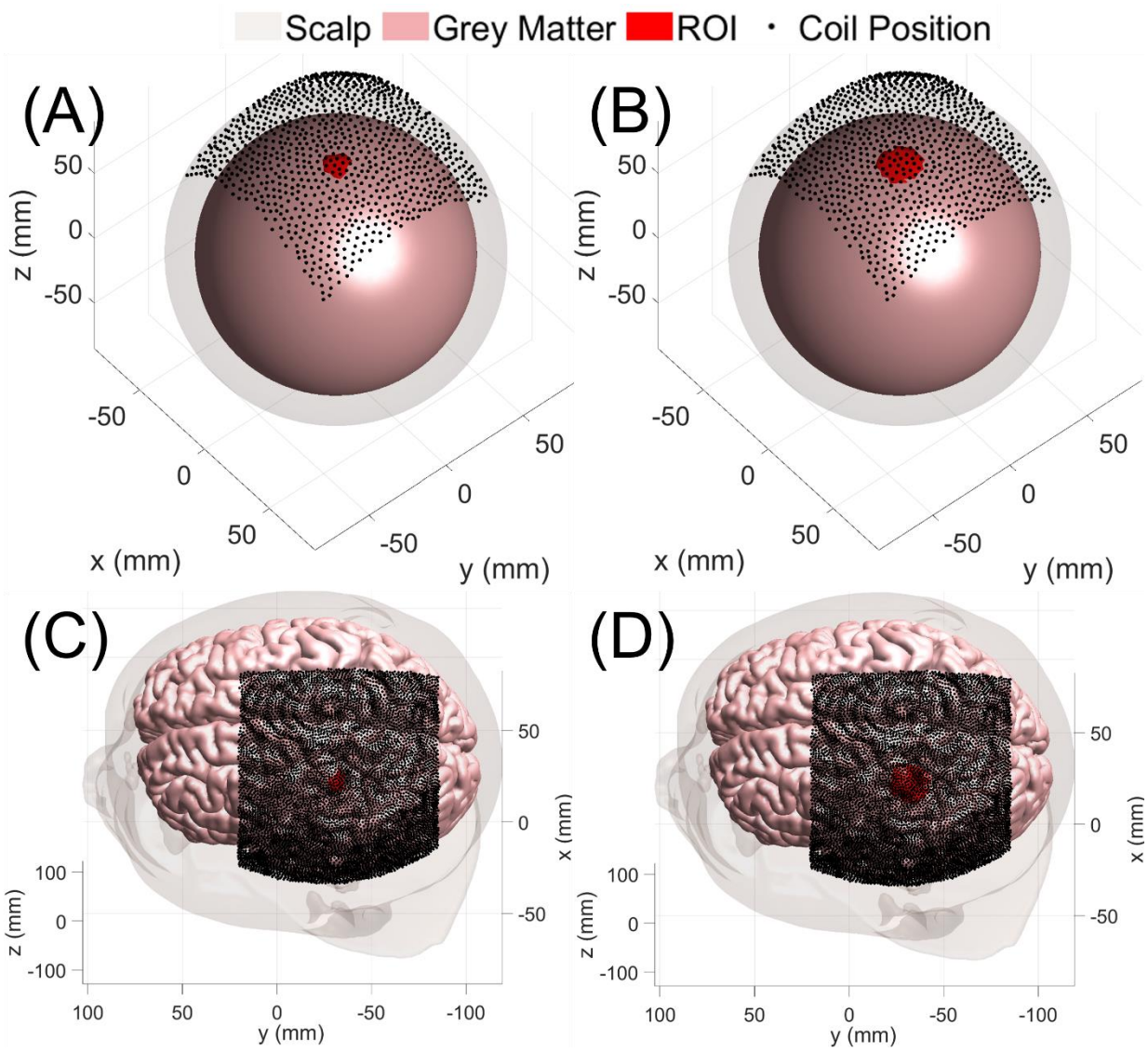

Fig. S1: ROIs and coil positions for the cases in Fig. 2

S.2 Details of the 162 ROIs

The 162 ROI center locations were chosen based on the 10-20 EEG system. However, the conventional 10-20 EEG system only contains 80 electrode positions (some of them cannot be used in our case). Therefore, we increase the resolution by adding around 100 more positions. The locations of the 162 positions on the cortex surface are shown in Fig. S2, and the detailed Cartesian coordinates are provided in Appendix Table SA1.

To investigate the stop criterion and rank requirement for different size ROIs, we studied the ROIs with diameters of 5, 10, 15, 20, …, 100 mm. Fig. S3 shows one example of the shape of the ROIs with different diameters (the 30th ROI center in Appendix Table SA1). The number of tetrahedra in each ROI are slightly different even for the same diameter. Fig. S4 provides the statistical distributions of the tetrahedra numbers in ROIs with different diameters, where Fig. S4-(A) shows the semilogy plot of all diameters, and (B) shows the linear plot of diameters $\geq$40 mm. The minimum, maximum and mean number of tetrahedra in ROIs with different diameters are given in Table S2.

The coil positions are chosen with the same strategy as that in S.1. The statistical distribution of number of coil positions for the 162 ROI centers is provided in Fig. S4. As can be seen, the number of coil positions ranges from 698 to 6,602, and most of the numbers cluster in the range of [4000,6500].

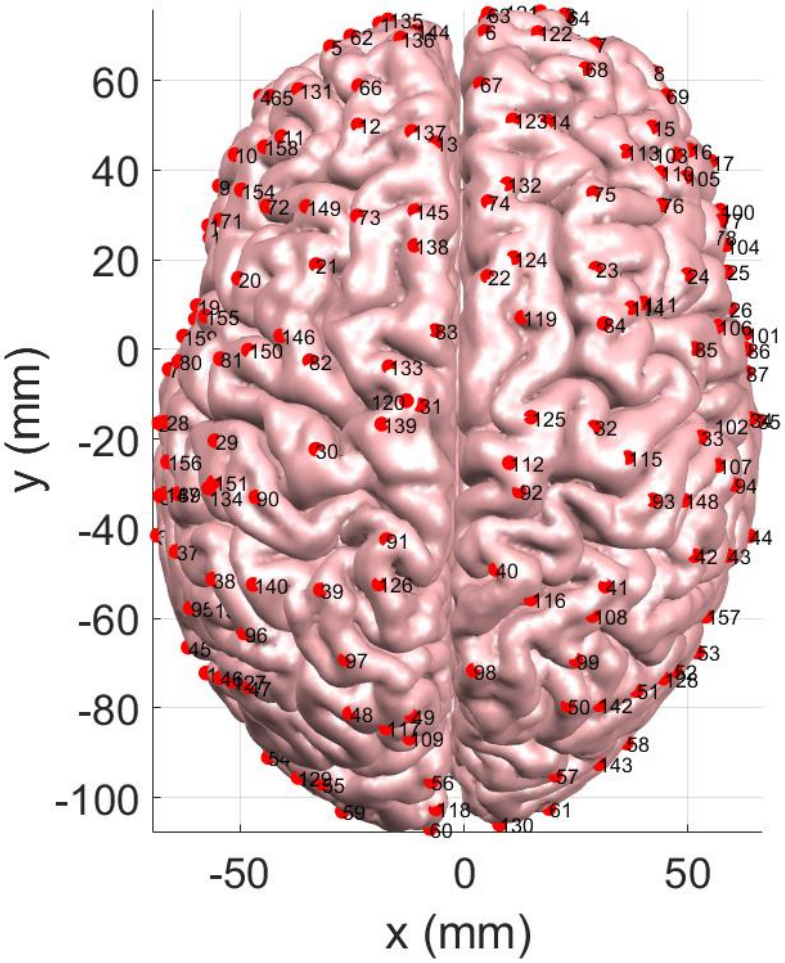

Fig. S2: Locations of the 162 ROI centers on the cortex surface

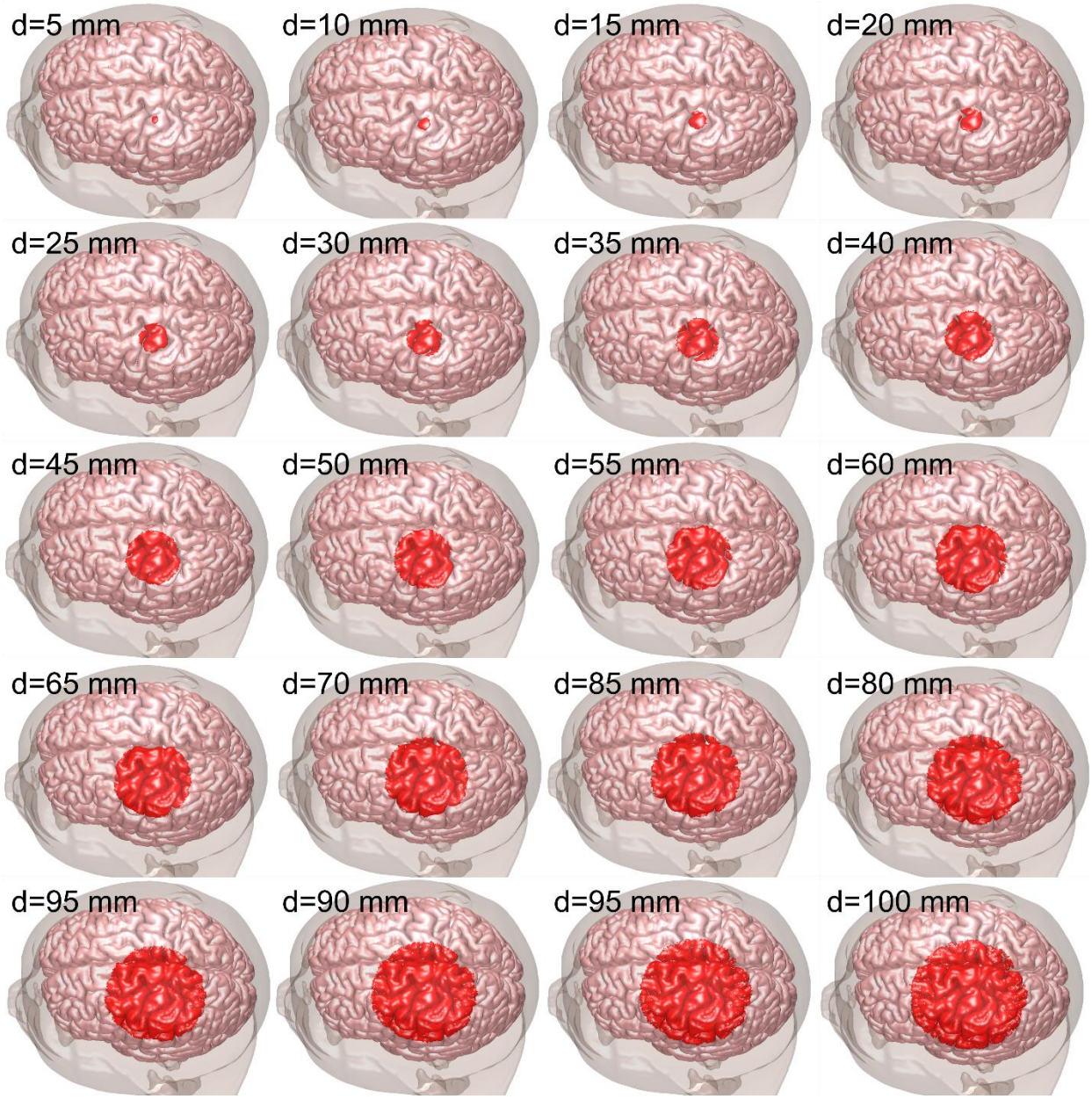

Fig. S3: ROIs with different diameters with center at (-33.1, -22.2, 91.2) mm.

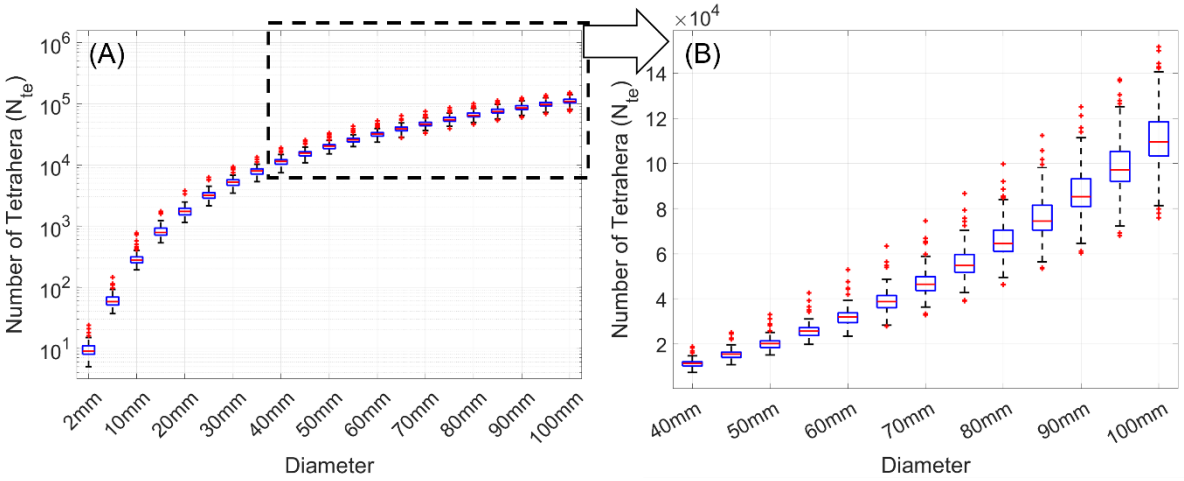

Fig. S4: Statistical distributions of the number of tetrahedra in the 162 ROIs with different diameters. (A) Semilogy plot for all diameters; and (B) Linear plot for diameters ≥40 mm.

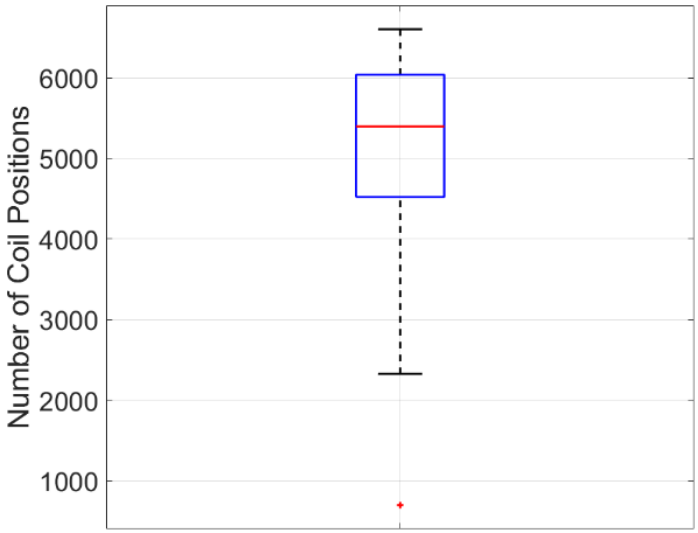

Fig. S5: Statistical distribution of the number of coil positions corresponding to the 162 ROI centers.

Table S2: Minimum, maximum and mean number of tetrahedra in the 162 ROIs with different diameters

Diameter (mm)	Minimum number	Maximum number	Mean number
2	5	24	9.6
5	37	146	61.5
10	192	769	293.6
15	531	1,727	831.4

20	1,146	3,760	1,772.0
25	2,147	6,215	3,213.4
30	3,452	9,258	5,227.9
35	5,320	13,352	7,915.7
40	7,451	18,856	11,302.7
45	10,855	25,253	15,395.4
50	15,174	33,045	20,221.8
55	19,882	42,649	25,814.4
60	23,535	52,920	32,185.9
65	27,853	63,377	39,258.8
70	32,922	74,550	47,200.8
75	39,037	86,725	56,036.6
80	46,308	99,708	65,727.7
85	53,464	112,356	76,082.0
90	60,271	125,015	86,995.9
95	67,950	137,269	98,450.6
100	75,868	151,698	110,403.1

S.3 Details of ROI numbers and coil position numbers of nine head models

The details of the ROI tetrahedron numbers and coil position numbers of the nine head models used to evaluate the ranks required for whole (gray and white) matter as ROI are shown in Fig. S6. As can be seen, the number of ROI tetrahedra ranges approximately from 1.53 to 1.58 million, and the number of coil positions ranges from 21,358 to 25,895 (thus 7,688,880 to 9,322,200 coil placements). The distribution of the coil positions on each head can be found in Fig. S7.

The preprocessing time scales as cost per ACA iteration times rank of the approximation. For the whole head results the average time per ACA iteration was between 328 s and 354 s. The distribution of pre-processing times for the nine heads with different accuracy levels is given in Fig. S8. As can be seen, the pre-processing time to get a 2% accuracy ranged between 14.3 and 18.7 hours. We also provide the distribution of reconstruction times on a CPU and GPU in Fig. S9. As can be seen, the CPU run time for reconstructing a single coil placement ranged between 0.336 and 0.443 s (2 % accuracy), whereas the GPU run time only ranged between 6.6 and 8.5 ms.

In this paper, we used 2.90 GHz Intel(R) Core(TM) i7-10700 CPU and Nvidia GeForce RTX 3080 GPU.

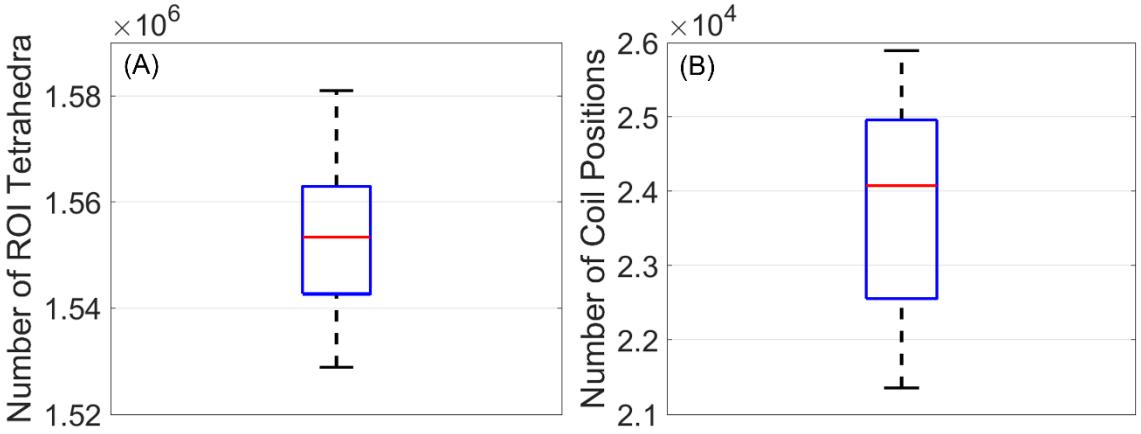

Fig. S6: Statistical distributions of the number of ROI tetrahedra and of coil positions. (A) Number of ROI tetrahedra; (B) Number of coil positions.

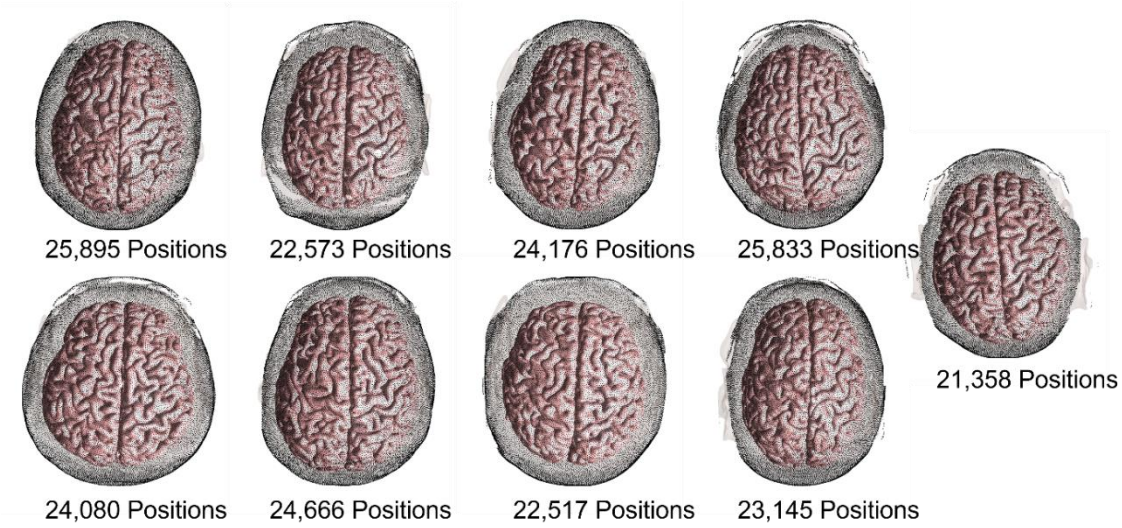

Fig. S7: The nine head models and the corresponding coil positions on each head (black points), where the number of coil positions are provided under each head.

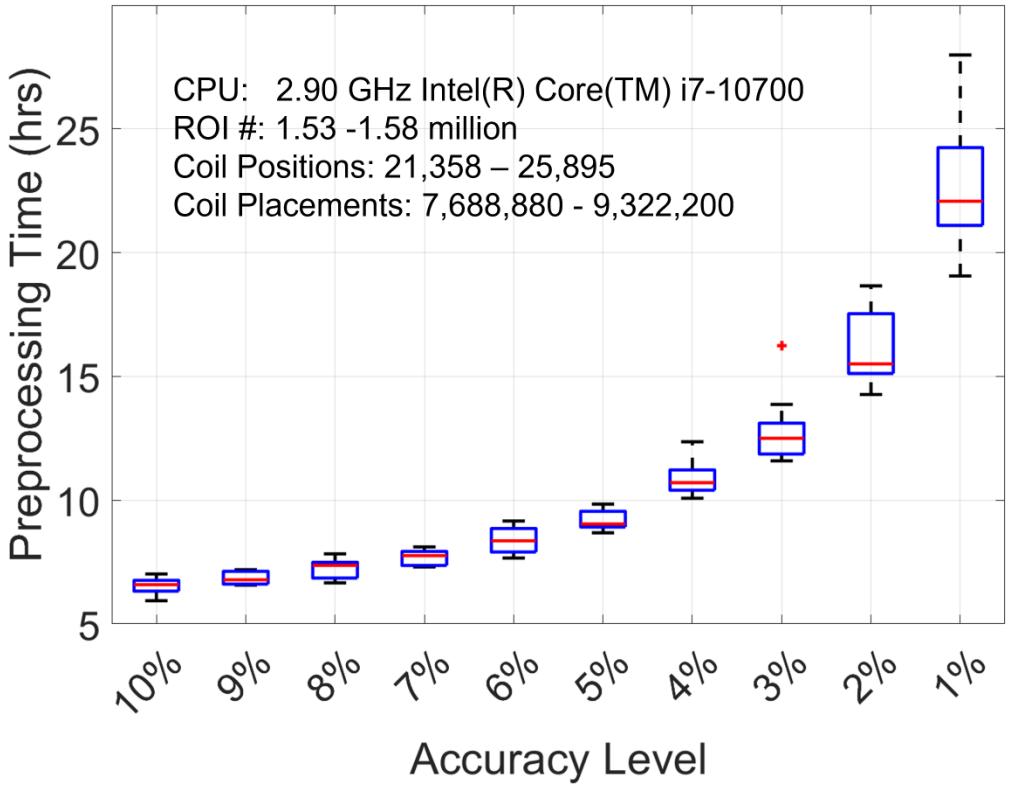

Fig. S8: Statistical distributions of pre-processing time for the nine heads with different accuracy levels.

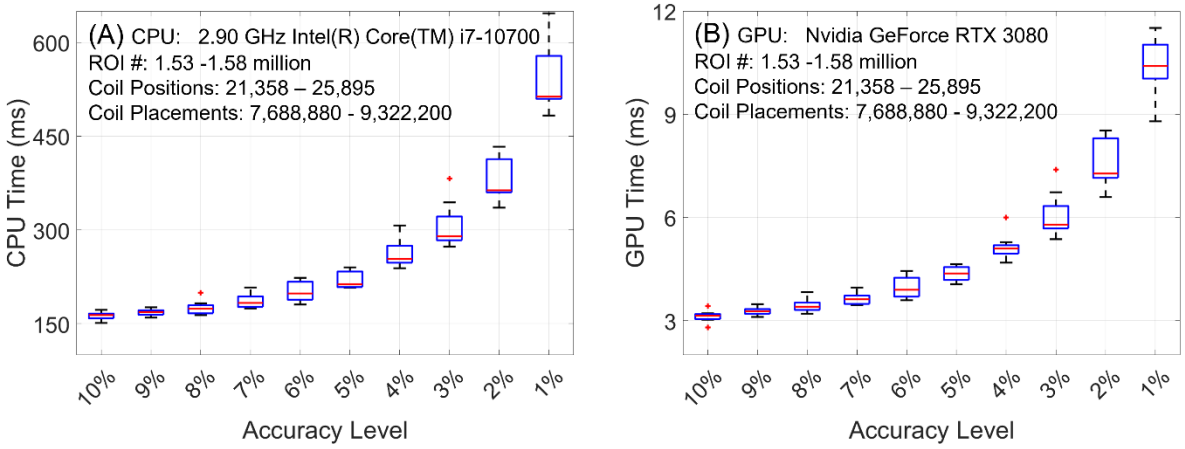

Fig. S9: Statistical distributions of reconstruction time for the nine heads with different accuracy levels on a CPU and GPU. (A) Reconstruction time on a CPU; (B) Reconstruction time on a GPU.

S.4 Details of reconstruction times

In the reconstruction stage, the E-field in the ROI from a certain coil placement is obtained by multiplying the obtained $\boldsymbol{U}^{(k)}$ with the column of $\boldsymbol{V}^{(k)}$ corresponding to the coil placement. In the analysis of the reconstruction time, we randomly chose 200 columns of $\boldsymbol{V}^{(k)}$ and respectively multiplied $\boldsymbol{U}^{(k)}$ with them for different ROIs with different diameters at 10%, 2% and 1% accuracy levels. The average time of each multiplication is recorded as the reconstruction time for that case. The statistical distributions of the 162 reconstruction times corresponding to 162 ROIs with different diameters at different accuracy levels are shown in Fig. S10 and S11, where Fig. S10 shows the semilogy plot for all diameters, while Fig. S11 shows the linear plot for diameters ≥40 mm.

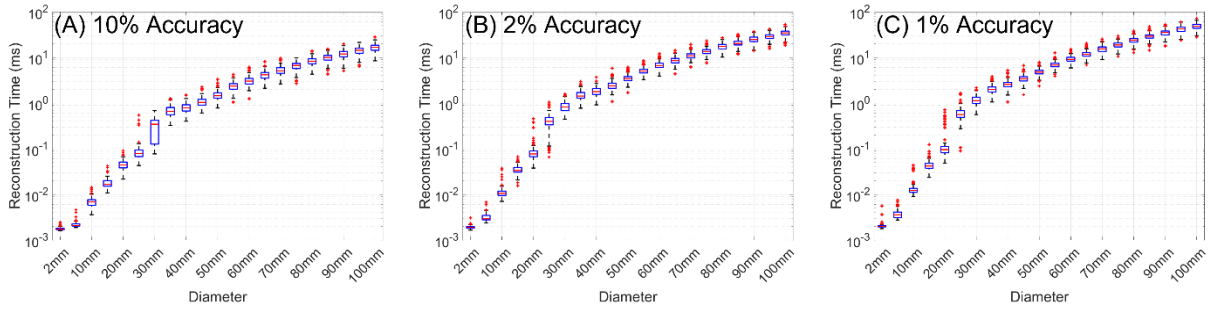

Fig. S10: Statistical distributions of the reconstruction time for different accuracy levels of the 162 ROI centers with different diameters (**semilogy plot**). (A) 10% accuracy; (B) 2% accuracy; and (C) 1% accuracy.

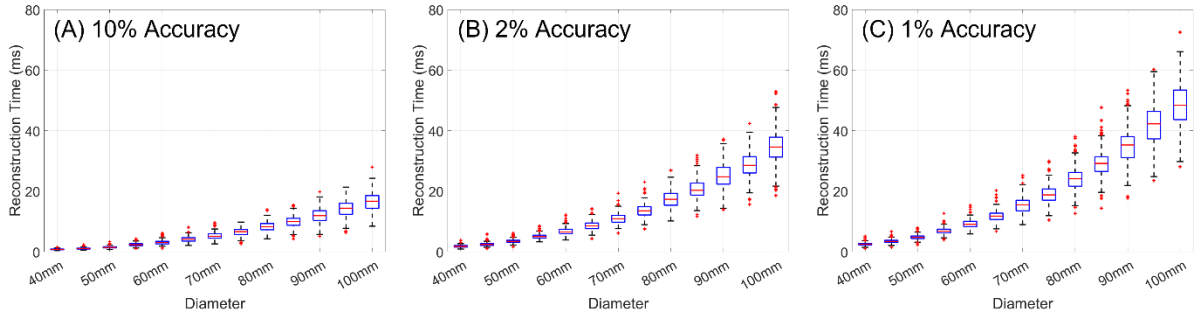

Fig. S11: Statistical distributions of the reconstruction time for different accuracy levels of the 162 ROI centers with diameters≥40 mm (**linear plot**). (A) 10% accuracy; (B) 2% accuracy; and (C) 1% accuracy.

Appendix

Here we provide the details of the location of the 162 ROI centers in Cartesian coordinate.

Table SA1: Details of the location of the 162 ROI centers in Cartesian coordinate

index	x(mm)	y(mm)	z(mm)	index	x(mm)	y(mm)	z(mm)	index	x(mm)	y(mm)	z(mm)
1	-18.9	72.8	37.2	**55**	-31.6	-96.8	36.8	**109**	-12.2	-86.7	64.5
2	4.8	73.3	39.3	**56**	-7.3	-96.4	46	**110**	43.8	39.5	64.7
3	22.5	74.7	40.4	**57**	20.4	-95	39.2	**111**	40	10.4	81.3
4	-45.4	56.5	31.8	**58**	36.2	-87.8	18.3	**112**	10.1	-25.3	99
5	-29.8	67.6	49.8	**59**	-27.1	-103.1	19.8	**113**	36	44.2	71.7
6	4.7	71	59.5	**60**	-7.6	-106.9	20.3	**114**	37.2	9.3	84.6
7	29.3	68.2	53.6	**61**	18.9	-102.4	13.9	**115**	36.5	-24.1	90.2
8	42.2	62	31	**62**	-25.3	70	45.1	**116**	14.9	-55.7	90.3
9	-54.6	36.5	30.7	**63**	5.3	74.9	50.7	**117**	-17.4	-84.5	71.3
10	-51.1	43.5	46.4	**64**	23	74.1	42.3	**118**	-6.3	-102.5	28.9
11	-40.7	47.5	63.2	**65**	-43.1	56.5	44.9	**119**	12.9	7.2	90.5
12	-23.7	50.1	73.7	**66**	-23.5	58.8	66	**120**	-12.8	-11.4	98.8
13	-6.4	46.1	83	**67**	3.6	59.3	73.7	**121**	17	75.3	40.1
14	18.7	50.9	77.1	**68**	27.1	62.7	62.9	**122**	16.5	70.7	57.1
15	41.9	49.6	61.2	**69**	45.1	56.7	48.7	**123**	10.9	51.2	78.4
16	50.3	44.5	50.2	**70**	-54.5	31.9	29.2	**124**	11	20.5	91.9
17	55	42	29.1	**71**	-54.4	28.9	51.9	**125**	14.9	-15.1	97.7
18	-60	6.8	25.1	**72**	-44	32	67.3	**126**	-19	-52.3	94.5
19	-59.5	9.8	52.7	**73**	-23.8	29.8	85.3	**127**	-51.8	-74	50.7
20	-50.4	15.9	71.4	**74**	5.3	33	88.8	**128**	44.5	-73.3	51.7
21	-33	18.9	85.2	**75**	28.8	35	81.9	**129**	-37	-95.5	28.3
22	5.3	16.3	92.3	**76**	44.1	32.3	68.6	**130**	7.9	-106	16.9
23	29.4	18.1	87.7	**77**	57.3	28.8	47.7	**131**	-36.9	58	57.4
24	49.8	16.7	71.1	**78**	55.7	25.1	33.6	**132**	9.6	37	86.5
25	58.6	17.3	51.6	**79**	-65.8	-4.4	19.5	**133**	-16.8	-3.9	96.9
26	59.3	9.1	26.3	**80**	-63.7	-2.7	51	**134**	-56.9	-30.9	73.8
27	-68	-16.4	19.3	**81**	-54.4	-2.1	71.3	**135**	-16.9	73.6	38.7
28	-66.5	-16.2	49.9	**82**	-34.4	-2.5	89.9	**136**	-14.1	69.5	60.8
29	-55.6	-20.4	75.8	**83**	-6.4	4.2	95.4	**137**	-11.7	48.7	81.2
30	-33.1	-22.2	91.2	**84**	31.2	5.8	88.9	**138**	-11	23.2	90.9
31	-9.8	-12.4	98.2	**85**	51.4	0.2	73.5	**139**	-18.4	-16.6	97.8
32	29	-17.3	91.8	**86**	63.1	0	50.1	**140**	-47	-52.4	80.9
33	52.8	-19.5	74.5	**87**	63	-5.1	18.1	**141**	-57.6	-72.2	27.2
34	63.9	-15.4	49.7	**88**	-67.8	-32.7	34.3	**142**	30.1	-79.2	66.4

35	65.6	-15.9	24.9	**89**	-63.9	-32.2	63.2	**143**	30	-92.4	28.7
36	-68.4	-41.5	15.1	**90**	-46.4	-32.9	85.1	**144**	-10.8	71	47.9
37	-64.2	-45.1	47.8	**91**	-17.3	-42.4	96.3	**145**	-11	30.9	89.4
38	-56.1	-51.3	71	**92**	12.3	-31.6	97.6	**146**	-40.9	3.1	85.7
39	-32	-53.6	87.8	**93**	42.1	-33.6	86.9	**147**	-66.6	-32.1	51.3
40	7	-49.1	95.7	**94**	60.4	-30.2	62.4	**148**	49.1	-33.6	78.7
41	31.6	-52.8	86.2	**95**	-61.1	-57.7	47.6	**149**	-35.2	31.9	76.8
42	51.4	-46	70.9	**96**	-49	-63.3	70.3	**150**	-48.1	-0.2	77.9
43	58.9	-46	49.1	**97**	-26.5	-69.1	83.9	**151**	-55.9	-29.6	74.8
44	63.7	-41.6	17.4	**98**	2.1	-71.6	83.2	**152**	-55.7	-57.9	53.2
45	-61.5	-66.4	17.9	**99**	25	-69.3	79.4	**153**	44.3	-35.3	-19.1
46	-54.4	-73.3	42.4	**100**	57.1	31.1	42.7	**154**	-49.7	35.6	56.2
47	-47.9	-75.3	56.8	**101**	62.8	3.5	47	**155**	-57.7	7.4	59.6
48	-25.5	-81.2	71.7	**102**	55.7	-16.8	51	**156**	-66.1	-25	56.9
49	-11.7	-81.7	74.9	**103**	47.2	43.6	57.1	**157**	54	-59.5	35.4
50	23.2	-79.4	71.2	**104**	58.4	23.3	46	**158**	-44.5	45.2	59
51	38.5	-76.1	59.8	**105**	49.5	38.5	57.7	**159**	-62.6	3	47.4
52	47	-71.6	41.8	**106**	56.7	5.2	64	**160**	-57	27.7	38
53	52.1	-67.5	20.1	**107**	56.7	-25.9	68.6	**161**	-53.9	1.4	32.5
54	-43.6	-91	14.8	**108**	28.7	-59.4	84.2	**162**	-56.7	24.9	36.9

Reference

[1] L. J. Gomez, M. Dannhauer, and A. V. Peterchev, “Fast computational optimization of TMS coil placement for individualized electric field targeting,” *Neuroimage*, vol. 228, p. 117696, 2021.